*Desalination and Water Treatment*
www.deswater.com

doi: 10.5004/dwt.2023.29739

302 (2023) 184–194
August

# $MoO_3$ adsorption kinetics and isotherm study with varied dye concentration

Naresh Kumar[a], Jaspreet Kaur[a], Surbhi Sharma[a], Jitendra Gangwar[b], Rajesh Kumar[a,*]

[a]*Department of Physics, Panjab University, Chandigarh 160014, India, emails: rajeshphysicspu@gmail.com (R. Kumar), naresh77352@gmail.com (N. Kumar), jk2471216@gmail.com (J. Kaur), surbhi241sharma@gmail.com (S. Sharma)*
[b]*Department of Physics, RPS Degree College, Balana, Mahendergarh, Haryana 123029, India, email: njitendrag127@gmail.com*

Received 20 November 2022; Accepted 22 June 2023

**ABSTRACT**

The effect of varying methylene blue dye concentrations on the adsorption activity of molybdenum oxide nanostructures has been investigated. The removal percentage and maximum adsorption efficiency were determined by varying the dye concentration from 20 to 150 mg/L. The adsorption rate constants, nature and type of adsorption were determined using pseudo-first-order, pseudo-second-order, and intraparticle diffusion kinetics models. Four different isotherm, that is, Langmuir, Freundlich, Temkin and Dubinin–Radushkevich models were used to understand the interaction of the adsorbate–adsorbent at interface and to calculate maximum adsorption efficiency. The mixed phase shows adsorption efficiency of 633.1 mg/g while orthorhombic phase gives much lesser efficiency, that is, 425 mg/g. The removal percentage decreases from 99% to 25.8% (orthorhombic phase) and 99.4% to 67.8% (mixed phase) with increasing dye concentrations.

*Keywords:* $MoO_3$; Structural phase; Mixed-phase; Adsorption; Methylene blue; Kinetics; Isotherm; Adsorption efficiency

## 1. Introduction

Organic dyes are complex chemicals that can be dangerous if dumped into water bodies without sufficient treatment. Large-scale industrialization has raised the use of dye-laden chemicals in manufacturing [1,2]. Following their use, these dye-infused substances are directly disposed into the environment, affecting flora and animals. These effluents in water increase chemical oxygen demand, impair visibility, and limit photosynthesis, impacting both people and aquatic life [3,4]. Here are some common types of dyes and their potential effects on human health. Synthetic organic dyes: These dyes are widely used in the textile, food, and cosmetic industries. Azo dyes are part of synthetic dye. Some synthetic dyes leads to cancer, skin irritation, and allergic reactions on direct exposure. For example, the dye Sudan red has been found to cause cancer in laboratory animals, and the dye para-phenylenediamine is a common cause of allergic reactions.

- Natural dyes: Natural dyes are derived from minerals, plants, and animals. Although they are generally considered safe, some of them can cause skin irritation and allergic reactions in sensitive individuals.
- Food dyes: Food dyes are used to color a wide range of processed foods. Some food dyes like dye tartrazine has been associated with asthma and hives in sensitive individuals. Few commonly used food dyes are Quinoline Yellow, Carmoisine, Ponceau 4R and Patent blue V etc.
- Hair dyes: Hair dyes are used to color hair and are often made with synthetic dyes which can trigger increased risk of cancer, particularly bladder cancer and leukaemia.
- Medical dyes: Medical dyes are used to help diagnose and treat medical conditions. For example, contrast dyes are used in medical imaging to highlight blood vessels and organs. While medical dyes are generally considered safe, some people may have an allergic reaction to them [5–10].

* Corresponding author.

Among varieties of these colorful pollutants, methylene blue (MB) is a type of organic dye that is widely used in sectors such as paper, leather, cosmetics, cotton and medicine to color their goods while using huge amounts of water [3]. It is estimated that about $7 \times 10^5$ tones of dyestuff are produced annually by various industries and drain lots of volumes of dye laden sludge. This untreated sludge from industries is discharged into the biosphere thereby creating ecological imbalance leading to poisoning of water resources [4]. The MB dye has the potential to trigger eye irritation which can induce long-term harm to both human and animal eyes. When breathed, it can produce brief bouts of rapid or difficult breathing, whereas ingestion can result in nausea, vomiting, mental confusion, profuse sweating and methemoglobinemia [11]. As a result, immediate action is essential to address the issue. Since the previous several decades, scientists are working on various approaches for water purification utilizing distinct techniques such as filtration, flocculation, membrane-separation, adsorption, ion-exchange, and photodegradation [3,4,11–14]. Among these, adsorption is the most extensively utilized approach due to its flexibility and simplicity, cost-effective adsorbents, ease of separation and low toxicity [13,14].

Adsorption is a surface phenomenon that can be influenced by synthesis condition of the adsorbent. Several surface modifying agents such as surfactant, urea and pH affects structures and morphologies and thereby affecting surface properties. Similarly, the adsorbent dose, pH of the solution, temperatures of the reactive solution, contact time of adsorbate–adsorbent interface and the dye concentration are the few parameters that influence the adsorption at a large extent [15,16]. The requirement of such type of adsorbent is highly recommendable that can decontaminate the MB used water so that it can be utilized for wastewater treatment.

A significant variety of transition metal oxides have been thoroughly investigated for dye removal from aqueous solution, with $MoO_3$ being of particular interest due to its high adsorption efficiency, less toxicity and cost-effective production [17]. The $MoO_3$ nanostructures can be found in a variety of phases, including stable o-$MoO_3$ and metastable h-$MoO_3$, each with its own distinct structure. Both of these phases were synthesized via separate ways from $MoO_6$ octahedra. The stable o-$MoO_3$ nanostructure is composed of stacked $MoO_3$ nanostructures with extremely thin layers of connected and deformed $MoO_6$ octahedra [18]. Similarly, the metastable phase h-$MoO_3$ is synthesized using $MoO_6$ octahedra. The connection of $MoO_6$ zig-zag chains via the cis-position produced a tunnel hexagonal crystalline structure, which distinguishes h-$MoO_3$ from o-$MoO_3$. These tunnels might include intercalated hydroxyl groups or water molecules, which could influence the physicochemical characteristics of h-$MoO_3$ nanostructures [19]. For example, Chthambararaj et al. [20] hydrothermally synthesized h-$MoO_3$ and o-$MoO_3$ and found higher electrical conductivity for h-$MoO_3$ based on their intercalated ions. Similarly, Song et al. [21] found better photochromic properties of mixed phase $MoO_3$ as compared to o-$MoO_3$ which is attributed to the narrow band gap of mixed phase.

Herein, we have utilized these $MoO_3$ nanostructures for the adsorption of MB with different initial dye concentration. Three different kinetics models such as pseudo-first-order, pseudo-second-order and intraparticle diffusion models have been employed for the determination of maximum adsorption efficiency and rate constants. Further, adsorbate–adsorbent interaction have been investigated by utilizing four different adsorption isotherm models such as Langmuir, Freundlich, Temkin and Dubinin–Radushkevich isotherm at three different temperatures. The major advantage of the present work is that adsorbent used are very much cost effective, higher removal and adsorption capacity, ecofriendly and reusable. However, the adsorption procedure inherits the problem of treating sludge using other methods like heat treatment or photocatalysis for degradation of dyes. The novelty of the work is that mixed-phase $MoO_3$ have not been studied for dye adsorption to the best of our knowledge. This mixed-phase behaviour may lead to extraordinary synergistic effect of different transition metal oxide phases and properties could be tunable as per requirement of the applications.

## 2. Experimental set-up

### 2.1. Materials, method and characterization

Ammonium heptamolybdate tetrahydrate (AHM), a AR grade product of Rankem with purity ≥ 99.0% was used as precursor material for the synthesis of $MoO_3$ nanostructures. The DI water, methanol (Honeywell, AR grade, purity ≥ 99.9%, Wunstorfer Strasse 40, D-30926 Seelze, Germany) and ethanol (CSS, AR grade, purity = 99.9%) were used as solvents. Urea (Qualigens, purity 99% , Thermo Fisher Scientific India Pvt., Ltd., 403-404, Delphi, B Wing, Powai, Hiranandani Business Park, Maharashtra 400076) was utilized as a fuel material during the synthesis of nanostructures. The detailed synthesis procedure was reported in previous article [22] where three different phases of $MoO_3$ were obtained. The h-$MoO_3$ was obtained with water as a solvent in acidic solution with pH 6, o-$MoO_3$ was obtained with methanol solvent and mixed phase (mp-$MoO_3$) was obtained by employing water/ethanol mixture as solvent. The synthesized materials were subjected to various characterization techniques for the structural and morphological studies. The hexagonal nanorod for h-$MoO_3$, orthorhombic layered nanosheets for o-$MoO_3$ and nanosheets for mp-$MoO_3$ were obtained. Moreover, the surface charge, surface area and pore volume was found to be highest for mp-$MoO_3$ followed by o-$MoO_3$ and h-$MoO_3$ [22].

### 2.2. Adsorption study

Different parameters such as adsorbent dose, pH of the solution, contact time and temperature of the reaction medium have been employed against MB adsorption and found the effectiveness of the adsorbent in our previous study [22]. The effect of initial dye concentration has been studied in this article because increasing adsorbate concentration also affects the adsorption phenomenon because of the enhancement of the adsorbing molecules. Here, 10 mg has been chosen as optimum adsorbent dose, temperature of the solution at 30°C and pH of the solution at 7. The initial dye concentration was varied from 20 to 150 mg/L and 40 mL solution was taken during the whole experimentation. The whole experimentation was done at constant stirring

rate on a magnetic stirrer. Subsequently to the addition of adsorbent into the contaminated solution with different dye concentration, 2 mL sample was taken out at regular interval of time to study the relative decrement in the dye concentration by utilizing the UV-Vis spectra using UV-Lambda 3000 spectrophotometer. The whole experimentation was performed in controlled dark environment to avoid the effect of stray light. The removal percentage ($R$%) and the maximum adsorbed efficiency ($q_t$, mg/g) at a particular time has been calculated using Eqs. (1) and (2) [23]:

$$R\% = \frac{C_o - C_f}{C_o} \times 100 \quad (1)$$

$$q_t = \frac{C_o - C_f}{w} \times V \quad (2)$$

where $C_o$ (mg/L) and $C_f$ (mg/L) are the initial and final concentration of the dye solution, $V$ is the volume of the solution in liters and $W$ is the weight of the adsorbent materials in grams (g). Further, the adsorption mechanism has been explored in detail with the help of various kinetics such as pseudo-first-order, pseudo-second-order and intraparticle diffusion models. The implication of the kinetics study determines that whether the physical, chemical or diffusion phenomenon dominated the removal of MB. Various isotherm models were employed at three different temperatures (30°C, 45°C and 60°C) to fully understand the interaction at the adsorbate–adsorbent interface and to maximize the adsorption efficiency. A regeneration study of the adsorbent was performed to check the ability of the material for multiple batch adsorption process. The adsorption process, the mechanism of adsorption and the regeneration has been depicted in Fig. 1.

## 3. Results and discussion

### 3.1. Adsorption equilibrium study

Fig. 2 shows the removal percentage as a function of contact time and initial dye concentration for $MoO_3$ nanostructures. Fig. 2A shows that with increasing initial dye concentration, the $R$% decreases continuously for h-$MoO_3$. Approximately 28% dye was removed in case of 20 mg/L initial dye concentration in 300 min which was reduced to only 4% at 150 mg/L dye concentration. The h-$MoO_3$ is thus exhibits low adsorption efficiency. It has been observed from Fig. 2B and C that for 20 and 40 mg/L dye concentration, 99.9% adsorption was occurred for both o-$MoO_3$ and mp-$MoO_3$ samples but o-$MoO_3$ takes longer time than mp-$MoO_3$. For o-$MoO_3$, as the initial concentration was increased from 20 to 150 mg/L, the initial rate of adsorption decreases because removal percentage was decreased. For 60 to 150 mg/L concentrations, small increase in removal percentage was observed in the time interval from 20 to 200 min. But after 200 min, sharp increase in removal percentage occurred. This is due to the diffusion of dye molecules after a particular time of interval. The highest removal percentage was observed for 20 and 40 mg/L concentration whereas smallest was observed for 150 mg/L.

The data represented in Table 1 shows that increasing dye concentration have reduced the adsorption efficiency. The maximum adsorption efficiency first increases with concentration and reaches to 425 mg/g for 80 mg/L but after that it starts decreasing with further increase in concentration. Similar is the case for mp-$MoO_3$ where removal efficiency decreases with rise in initial dye concentrations. The maximum adsorption efficiency of mp-$MoO_3$ was found for 120 mg/L dye concentration with a value of 633.1 mg/g. However, the comparison of two samples show that mp-$MoO_3$ is an efficient adsorbent as compared to o-$MoO_3$ since it shows higher removal efficiency than o-$MoO_3$ for the studied dye concentrations. A common trend was found in both the samples that initial adsorption rate was higher in both cases but after 20 min, a plateau type behaviour was observed with very small increase in $R$%. But after 100 or 120 min, the rate increases drastically for higher dye concentration. This behaviour is attributed to the mechanism that with increasing dye concentration, the adsorption sites was occupied easily by the dye molecules through physical or chemical interaction. Once all the surface sites get

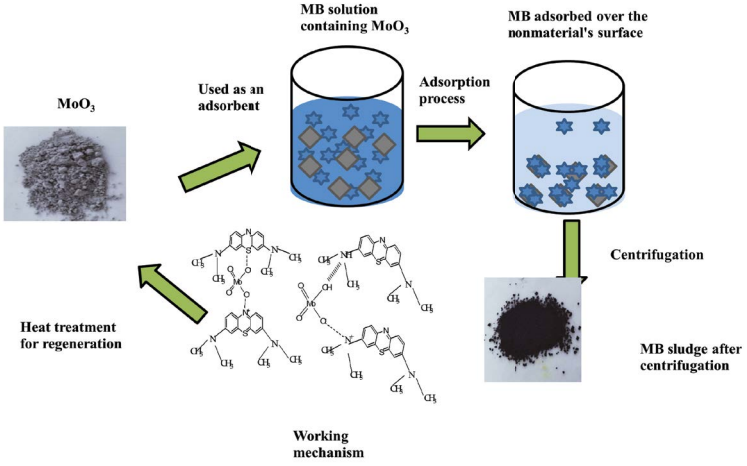


Fig. 1. Schematic representation of adsorption and desorption process.

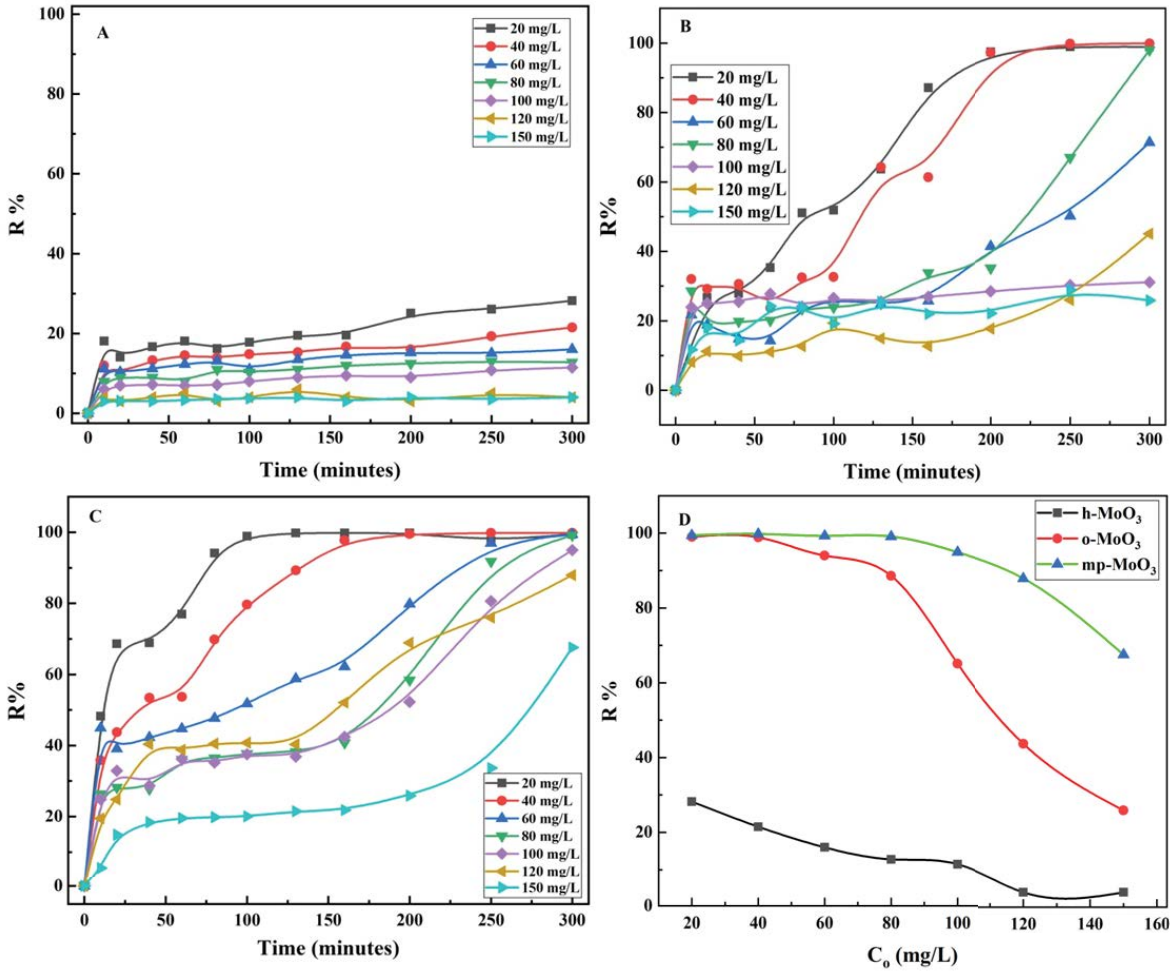


Fig. 2. *R*% as a function of contact time with various initial dye concentration for (A) h-$MoO_3$, (B) o-$MoO_3$ and (C) mp-$MoO_3$. The *R*% as a function of initial dye concentrations is depicted in Fig. 2D.

occupied, the adsorption process get slower for the additional dye molecules. Since the stirring continues, some dye molecules attaches as well detaches in the mean time. After a particular time interval (almost 200 min in o-$MoO_3$ and 160 min in mp-$MoO_3$) diffusion of dye molecules occurred into the adsorbent and thereby the adsorption process again getting faster kinetics. To further understand the adsorption phenomenon, kinetics study was performed using various kinetic models.

### 3.2. Adsorption kinetics

The adsorbate–adsorbent interaction and adsorption mechanism were studied by modeling the experimental data with different kinetic models [24]. The non-linear pseudo-first-order model described as Eq. (3):

$$q_t = q_e\left(1 - e^{-k_1 t}\right) \tag{3}$$

where $q_e$ (mg/g) is the removal capacity at equilibrium, $q_t$ (mg/g) is the removal capacity at time t, and $k_1$ (1/min) is a kinetic rate constant for pseudo-first-order model. Whereas pseudo-first-order model suggest the physical transfer of the adsorbate molecule at the adsorbent single active site [25], the pseudo-second-order kinetics relates the adsorption to be chemical interaction at the interface involving electrostatic interaction [26]. The pseudo-second-order kinetics model is described as Eq. (4):

$$q_t = \frac{q_e^2 k_2 t}{q_e k_2 t + 1} \tag{4}$$

where $q_e$ (mg/g) denotes removal capacity at equilibrium, $q_t$ (mg/g) represents the removal capacity at time t, and $k_2$ (g/mg·min) is the pseudo-second-order kinetic rate constant. Similarly, the intraparticle diffusion model was used to investigate the possibility of solute diffusion into the adsorbent layers. The intraparticle diffusion model was applied as a piecewise linear graph to fit the experimental data. The intraparticle diffusion model is described as given below [25,26]:

$$q_t = k_i t^{0.5} + C \tag{5}$$

Table 1
Removal percentage and maximum adsorption efficiency for o-$MoO_3$ and mp-$MoO_3$ nanostructures (10 mg adsorbent dose, pH 7, contact time 300 min and temperature 30°C)

| Sample | $C_o$ (mg/L) | $R$% | $Q_{exp}$ (mg/g) |
|---|---|---|---|
| o-$MoO_3$ | 20 | 99.0 | 118.6 |
| | 40 | 98.9 | 237.4 |
| | 60 | 94.0 | 338.4 |
| | 80 | 88.6 | 425.0 |
| | 100 | 65.1 | 390.8 |
| | 120 | 43.7 | 314.6 |
| | 150 | 25.8 | 232.8 |
| h-$MoO_3$ | 20 | 28.2 | 33.8 |
| | 40 | 21.5 | 51.6 |
| | 60 | 16 | 57.6 |
| | 80 | 12.8 | 61.4 |
| | 100 | 11.5 | 69.0 |
| | 120 | 4 | 28.8 |
| | 150 | 4 | 36.0 |
| mp-$MoO_3$ | 20 | 99.4 | 119.3 |
| | 40 | 99.8 | 239.5 |
| | 60 | 99.3 | 357.7 |
| | 80 | 99.1 | 476.0 |
| | 100 | 94.9 | 569.8 |
| | 120 | 87.9 | 633.1 |
| | 150 | 67.5 | 608.1 |

where C (mg/g) and $k_i$ (mg/g·$min^{0.5}$) are intraparticle diffusion constants, $q_t$ (mg/g) is the removal capacity at time t, and t (min) is the contact time.

Fig. 3A–C show the pseudo-first-order, pseudo-second-order and intraparticle diffusion kinetics models fitted to the experimental data of o-$MoO_3$ nanostructures. The calculated kinetic parameters are summarized in Table 2a. For the lowest and highest values of dye concentration under study, the correlation coefficient was found to be better than the intermediate values for both pseudo-first-order and pseudo-second-order models. It is attributed to the physical as well as chemical interaction at the interface. The maximum adsorbed amount was not found to be in close agreement to the experimental value in both cases of pseudo-first-order and pseudo-second-order. Therefore, intraparticle diffusion model was employed to the experimental data and result is shown in Fig. 3C. The experimental data are well fitted with the intraparticle diffusion model. It was observed that initial adsorption occurs due to the presence of negative charge and bare specific surface area of the adsorbent. For higher concentrations, a plateau type region was obtained at second step which hints that all the sites are occupied and no adsorption occur thereafter through physical or chemical process. But after certain time, the rate of adsorption became extremely fast which suggest the diffusion of dye molecules into adsorbent. Thus, with varying concentration of dye, diffusion of dyes have occurred along with physical and chemical interaction at the interface.

Similar to o-$MoO_3$, the kinetics study corresponding to mp-$MoO_3$ nanostructures are represented in Fig. 3D–F. The parameters have been calculated and summarized

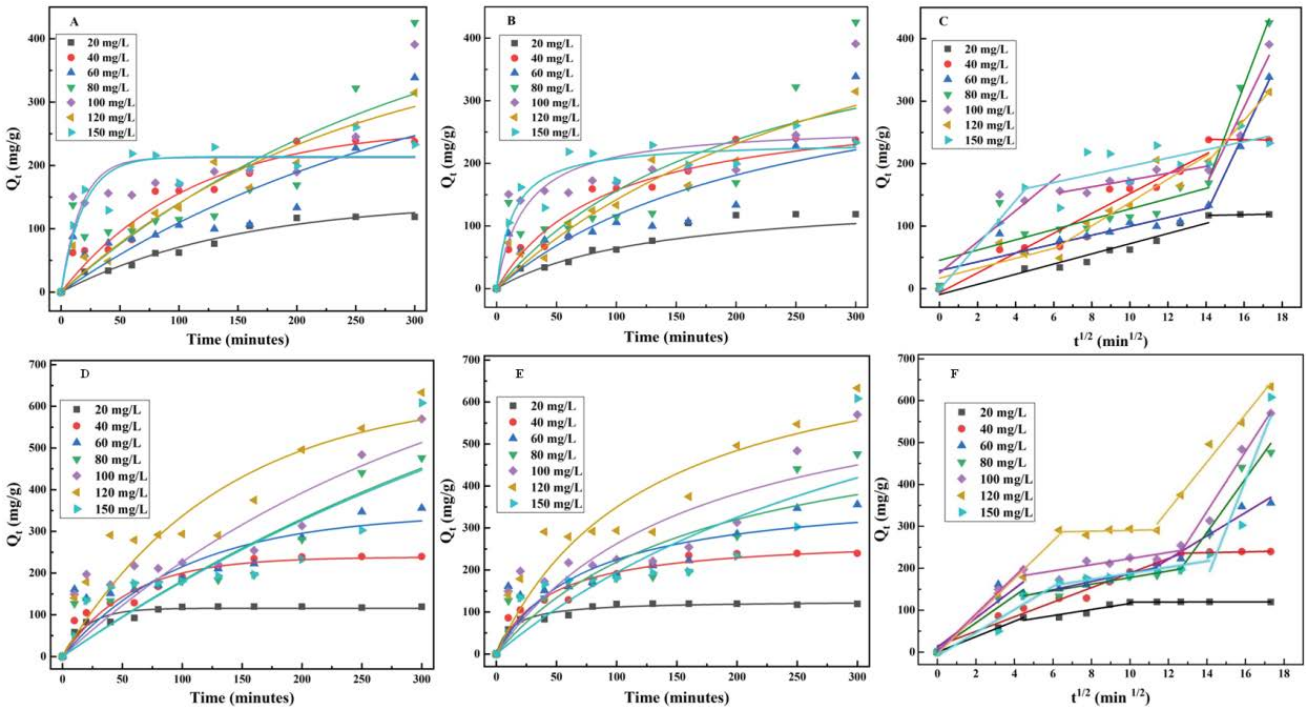


Fig. 3. Non-linear pseudo-first-order, pseudo-second-order and intraparticle diffusion kinetics plots for o-$MoO_3$ (A–C) and mp-$MoO_3$ (D–F) nanostructures, respectively with varying initial dye concentrations.

in Table 2a and found that the maximum adsorption efficiency is in well agreement to pseudo-first-order except for 150 mg/L concentration of dye. The maximum adsorption efficiency using mp-$MoO_3$ was found to be 633.1 mg/g experimentally and 632.5 mg/g theoretically. Although maximum adsorbed efficiency was not in well agreement to pseudo-second-order kinetics but the pseudo-second-order kinetics rate constant suggest that increasing dye concentration have slowed the process as highest rate constant was found for 20 mg/L and lowest for 150 mg/L.

Further, intraparticle diffusion model was applied to the experimental data and found that adsorption occurred via following three steps. As mentioned earlier, the initial rate was little bit higher, but in the intermediate time, a saturation like stage was reached. But after a particular time, again the rate becomes faster and adsortion occured via diffusion of dye molecules. The data suggest that mp-$MoO_3$ is a better adsorbent materials as compared to o-$MoO_3$ nanostructures since it is giving high adsorption efficiency. The corresponding derived parameters are summarized in Table 2b.

### 3.3. Adsorption isotherm

The thermodynamic equilibrium set up between solute adsorbed over the adsorbent surface with the remaining amount of adsorptive in the solution represented graphically using adsorption isotherms [27]. Therefore, four

Table 2a
Kinetics parameters corresponding to pseudo-first-order and pseudo-second-order using $MoO_3$ nanostructures

| Adsorbent | $C_o$ (mg/L) | $Q_{exp}$ (mg/g) | Pseudo-first-order | | | Pseudo-second-order | | |
|---|---|---|---|---|---|---|---|---|
| | | | $Q_{th}$ (mg/g) | $k_1$ (min$^{-1}$) | $R^2$ | $Q_{th}$ (mg/g) | $k_2$ (g/mg·min) | $R^2$ |
| | 20 | 118.6 | 144.6 | 0.00672 | 0.9606 | 130 | 0.000105 | 0.8722 |
| | 40 | 237.4 | 261.1 | 0.00906 | 0.9316 | 270 | 0.000036 | 0.9213 |
| | 60 | 338.4 | 400 | 0.00320 | 0.6872 | 380 | 0.0000103 | 0.6358 |
| o-$MoO_3$ | 80 | 425.0 | 500 | 0.00328 | 0.6605 | 500 | 0.0000090 | 0.6014 |
| | 100 | 390.8 | 212.5 | 0.05908 | 0.4206 | 261.1 | 0.000157 | 0.5366 |
| | 120 | 314.6 | 408.9 | 0.00420 | 0.9099 | 622.2 | 0.0000047 | 0.9134 |
| | 150 | 232.8 | 213.6 | 0.05259 | 0.8164 | 235.3 | 0.0003167 | 0.8565 |
| | 20 | 119.3 | 115.6 | 0.05008 | 0.9294 | 126.4 | 0.0006006 | 0.9661 |
| | 40 | 239.5 | 238.3 | 0.01824 | 0.9223 | 278.2 | 0.000083 | 0.9469 |
| | 60 | 357.7 | 342.8 | 0.00987 | 0.6671 | 390.5 | 0.000034 | 0.7183 |
| mp-$MoO_3$ | 80 | 476.0 | 490 | 0.00528 | 0.7364 | 550 | 0.000019 | 0.7110 |
| | 100 | 569.8 | 600 | 0.00471 | 0.6726 | 650 | 0.0000107 | 0.6850 |
| | 120 | 633.1 | 632.5 | 0.00760 | 0.8166 | 788.0 | 0.0000101 | 0.8427 |
| | 150 | 608.1 | 910 | 0.00210 | 0.6785 | 850 | 0.0000035 | 0.6551 |

Table 2b
Kinetics parameters corresponding to intraparticle diffusion kinetics

| Sample | Dye conc. (mg/L) | Intraparticle diffusion kinetic parameters | | | | | | | | |
|---|---|---|---|---|---|---|---|---|---|---|
| | | $C_1$ | $k_1$ | $R^2$ | $C_2$ | $k_2$ | $R^2$ | $C_3$ | $k_3$ | $R^2$ |
| | 20 | –9.61 | 8.13 | 0.9254 | 109.35 | 0.55 | 0.5494 | | | |
| | 40 | –6.71 | 15.85 | 0.9191 | 242.07 | –0.23 | 0.9501 | | | |
| | 60 | 28.60 | 7.08 | 0.7568 | –781.7 | 64.39 | 0.9880 | | | |
| o-$MoO_3$ | 80 | 45.13 | 8.22 | 0.5881 | –968.9 | 80.86 | 0.9867 | | | |
| | 100 | 24.73 | 24.96 | 0.6840 | 119.07 | 5.46 | 0.8092 | –714.23 | 62.78 | 0.8449 |
| | 120 | 16.65 | 7.94 | 0.1849 | –49.04 | 18.66 | 0.8138 | –287.58 | 34.80 | 0.9995 |
| | 150 | –1.71 | 35.62 | 0.9919 | 130.37 | 6.55 | 0.4379 | | | |
| | 20 | –0.05 | 18.39 | 0.9999 | 43.46 | 7.24 | 0.8071 | 118.75 | 0.053 | 0.9999 |
| | 40 | 14.56 | 17.37 | 0.9703 | 223.04 | 1.00 | 0.5752 | | | |
| | 60 | 11.46 | 34.92 | 0.6830 | 89.88 | 9.79 | 0.9222 | –112.14 | 27.80 | 0.9338 |
| mp-$MoO_3$ | 80 | 5.72 | 32.07 | 0.8944 | 99.05 | 7.86 | 0.8300 | –611.24 | 64.04 | 0.9365 |
| | 100 | 1.86 | 44.68 | 0.9943 | 149.73 | 7.33 | 0.6220 | –665.14 | 71.46 | 0.9617 |
| | 120 | –4.01 | 44.82 | 0.9836 | 280.51 | 0.98 | 0.9560 | –342.92 | 56.87 | 0.9713 |
| | 150 | –8.57 | 27.47 | 0.8891 | 114.80 | 7.29 | 0.8107 | –1458.5 | 116.75 | 0.7300 |

different isotherm, that is, Langmuir, Freundlich, Temkin and Dubinin–Radushkevich isotherms have been employed to determine the maximum dye adsorbed onto the surface at equilibrium time. The Langmuir isotherm model is expressed as Eq. (6) [28]:

$$q_e = \frac{q_m K_L C_e}{1 + K_L C_e} \tag{6}$$

where $q_e$, $C_e$, $q_m$, $K_L$ are the amount of adsorbed dye per gram of the adsorbent at equilibrium time in mg/g, the concentration of the MB in mg/L at the equilibrium, the maximum adsorption capacity in mg/g of the monolayer coverage and the Langmuir constant (L/mg), respectively. $K_L$ is characterized by the ability of the given surface to adsorb a given solute from the mixture with a given solvent. This isotherm assumes monolayer adsorption over the adsorbent surface containing homogeneous adsorption sites and therefore neglects the possibility of transmigration of the adsorbate in the adsorbent plane surface. So, if a particular site is occupied, no further adsorption can happen at that site and thereby a condition of saturation is achieved. The Freundlich adsorption isotherm on the other hand suggests the multilayer coverage of adsorbate at the adsorbent surface and expressed in Eq. (7) [29,30]:

$$q_e = K_F C_e^{1/n} \tag{7}$$

where $q_e$ (mg/g) adsorption capacity at equilibrium, $C_e$ (mg/L) equilibrium dye concentration, $K_F$ ($mg^{1-1/n}/L^{1/n}$·g) is the Freundlich constant and $n$ is the adsorption intensity.

The energy of molecular bonds in the adsorbents changes by the interaction at the adsorbate/adsorbent interface. The Temkin isotherm model assumes that the heat of adsorption does not remain constant in adsorbent–adsorbate interaction; rather it decreases due to the interaction between these two species and therefore explains the adsorption phenomenon. The non-linear form of Temkin isotherm is expressed as given in Eq. (8) [31,32]:

$$q_e = \frac{RT}{B_T} \ln\left(A_T C_e\right) \tag{8}$$

where $q_e$ (mg/g) is the adsorption capacity at equilibrium, $C_e$ (mg/L) is the equilibrium concentration of dye, $A_T$ gives information about the binding energy, $B_T$ is the heat of adsorption for a particular adsorption experiment, $R$ is the universal gas constant (8.3145 J/K·mol) and $T$ (K) is the temperature.

Compared to the Langmuir isotherm, the Dubinin–Radushkevich isotherm is more general since it does not presuppose a homogeneous surface or a constant sorption potential. The expression for Dubinin–Radushkevich isotherm is given in Eq. (9) [31,32]:

$$q_e = q_m e^{-B\left[RT\ln\left(1+\frac{1}{C_e}\right)\right]^2} \tag{9}$$

where $B$ ($mol^2/kJ^2$) is a constant related to the adsorption energy, $R$ (8.314 J/mol·K) is the gas constant, and $T$ (K) is the absolute temperature. The constant $B$ gives the mean free energy $E$ (kJ/mol) of sorption per molecule of the sorbate when it is transferred to the surface of the solid from infinity in the solution and can be computed using Eq. (10).

$$E = \frac{1}{\sqrt{2B}} \tag{10}$$

This parameter gives information about chemical or physical adsorption. With the magnitude of $E$, between 8 and 16 kJ/mol, the adsorption process follows chemical interaction, while for the values of $E$ < 8 kJ/mol, the process is of a physical nature [33].

Fig. 4A–C represent isotherm fitting corresponding to the o-$MoO_3$ adsorbent with different initial dye concentrations at three different temperatures. The parameters calculated using these isotherm models are summarized in Table 3. It has been found that for 30°C, the correlation coefficient was not good for all three isotherms but at higher temperature 45°C and 60°C, good $R^2$ values was found for Freundlich isotherm. The increasing temperature produces the new reactive sites and enhances the adsorption. The Freundlich constant was higher as compared to Langmuir constant which suggests that Freundlich isotherm may be the dominating mechanism at higher temperatures [28,29]. Literature reveals that a value of $1/n$ less than 1 stands for a less cooperative process whereas a greater than 1 value indicates the cooperative adsorption process [34]. The decrement in the $1/n$ value elaborate that adsorption becomes more heterogeneous. The values of $1/n$ are very close to each other and less than 1 ensures that adsorption is not very cooperative, heterogeneous and efficient at low MB concentrations. Comparing the data using Temkin isotherm clearly indicates that Temkin isotherm is not a dominating mechanism for adsorption process as poor $R^2$ coefficient was obtained. Further insight gained over adsorption mechanism was through Dubinin–Radushkevich isotherm which indicate that it is not a physical adsorption of dye as the derived mean free energy comes out to be greater than 8 kJ/mol. Although, for few cases, it deviates from the value because of the poor correlation coefficient [33]. Therefore, Freundlich isotherm favoring the heterogeneous adsorption is a dominating mechanism for adsorption using o-$MoO_3$ adsorbent.

The comparison of different adsorption isotherm at three different temperatures using mp-$MoO_3$ adsorbent is shown in Fig. 4D–F and calculated values are summarized in Table 3. It has been found that at low temperature, the data are well fitted to the Langmuir adsorption isotherm with good $R^2$ values. When the temperature is increased to 45°C, the Langmuir constant as well as adsorption efficiency increased. Further increase in temperature to 60°C again reduces the Langmuir constant as well as maximum adsorption efficiency which suggest that the higher temperature is not suitable for adsorption in case of mp-$MoO_3$ adsorbent. The adsorption efficiency at 30°C is well matched to the experimental data. The maximum monolayer adsorption efficiency was found to be 729.8 mg/g using Langmuir isotherm. It has been observed from Table 3 that at 30°C, the correlation coefficient for Freundlich isotherm was not good as compared to Langmuir isotherm but better than

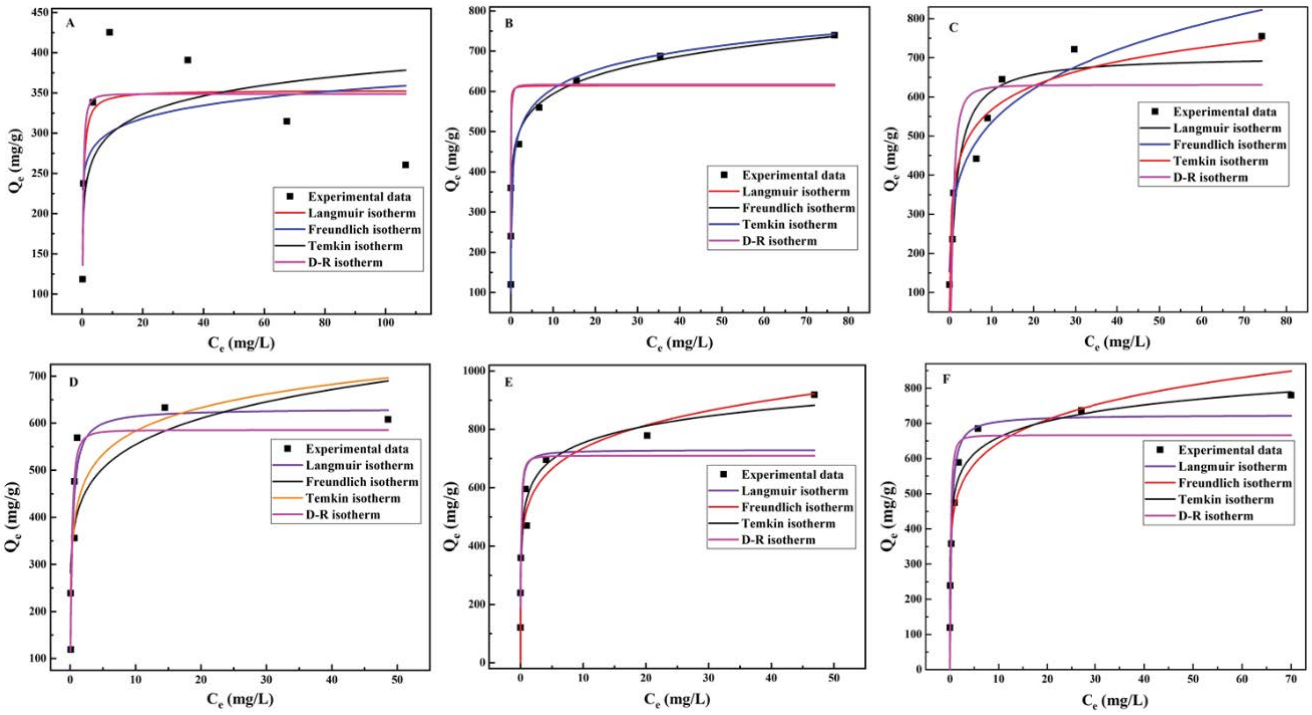


Fig. 4. Adsorption isotherm study using o-$MoO_3$ (A–C) and mp-$MoO_3$ (D–F) adsorbent at three different temperatures 30°C (A, D), 45°C (B, E) and 60°C (C, F) with contact time 300 min for 10 mg adsorbent dose at natural pH.

Table 3
Adsorption isotherm data corresponding to $MoO_3$ nanostructures

| | Adsorbent | o-$MoO_3$ | | | mp-$MoO_3$ | | |
|---|---|---|---|---|---|---|---|
| | Temp. (°C) | 30 | 45 | 60 | 30 | 45 | 60 |
| Langmuir isotherm | $q_m$ (mg/g) | 353.3 | 614.6 | 705.3 | 630.7 | 729.8 | 724.4 |
| | $K_L$ (L/mg) | 3.573 | 85.82 | 0.6757 | 3.754 | 12.22 | 3.556 |
| | $R^2$ | 0.6174 | 0.78 | 0.8599 | 0.8489 | 0.7609 | 0.8782 |
| Freundlich isotherm | $n$ | 13.9 | 9.43 | 4.64 | 7.24 | 6.82 | 7.06 |
| | $1/n$ | 0.07 | 0.1 | 0.21 | 0.13 | 0.15 | 0.14 |
| | $K_F$ | 256.5 | 464.9 | 325.3 | 403.3 | 524.4 | 466.2 |
| | $R^2$ | 0.1456 | 0.9368 | 0.9291 | 0.594 | 0.9285 | 0.92 |
| Temkin isotherm | $A_T$ (L/mg) | 1,000 | 700 | 59.24 | 347.8 | 833.3 | 1,000 |
| | $B_T$ (J/mol) | 77.09 | 38.68 | 31.19 | 35.22 | 31.68 | 41.53 |
| | $R^2$ | 0.2988 | 0.6904 | 0.866 | 0.4961 | 0.9055 | 0.9131 |
| Dubinin–Radushkevich isotherm | $q_m$ (mg/g) | 348.6 | 617 | 630.7 | 585.4 | 709.7 | 666.6 |
| | $B$ (mol²/kJ²) | 0.00464 | 0.00051 | 0.01787 | 0.00326 | 0.00126 | 0.00251 |
| | $E$ (kJ/mol) | 10.38 | 31.31 | 5.28 | 12.38 | 19.92 | 14.11 |
| | $R^2$ | 0.5888 | 0.7574 | 0.719 | 0.7457 | 0.6945 | 0.7583 |

Temkin model. The increase in temperature have improved the $R^2$ values for Freundlich isotherm and found to be better than other models. So, at higher temperature heterogeneous sites are created due to bond breakage or internal molecular motion. Moreover, the mean free energy calculated using Dubinin–Radushkevich isotherm hints towards chemical interaction occurring at the interface which is not completely assured as correlation coefficient is not much good as compared to Freundlich isotherm. Overall, it can be said that multilayer adsorption has occurred over the adsorbents surface. Here, adsorption increases with increase in temperature but further increase in temperature causes the reduction in the adsorption efficiency again. The maximum adsorption efficiency corresponding to various adsorbents employed for MB adsorption is summarized in Table 4. The parameters in Table 4 suggest that o-$MoO_3$ and mp-$MoO_3$ are

better suitable metal oxides for the adsorptive removal of MB dye.

### 3.4. Regeneration study

Adsorption plays a vital role for the wastewater treatment practically if the regeneration of adsorbent is efficient and the regeneration ability is high. For this 10 mg of all three $MoO_3$ nanostructures have been employed for regeneration study with 20 mg/L dye concentration at natural pH (pH 7) with 30°C temperature for a contact time of 300 min. After first cycle of adsorption, the supernatant was centrifuged and collected sludge was heat treated at 250°C temperature for 2–3 h. Due to this heat treatment, the dye gets desorbed and removed from the surface. The synthesis of $MoO_3$ nanostructures was done at 300°C temperature, therefore in regeneration study the temperature was kept below that temperature to avoid any structural changes of the materials. The regenerated material again employed for second and third cycles and data has been collected. Fig. 5 shows the *R*% corresponding to 3 cycles. It has been observed that there is slight change in the removal activity in case of o-$MoO_3$ and mp-$MoO_3$ nanostructures upto studied cycles but in case of h-$MoO_3$, a large reduction in the *R*% was observed. The results show that both o-$MoO_3$ and mp-$MoO_3$ can be good adsorbent by seeing their removal capacity and regeneration abilities.

Table 4
Maximum MB adsorption efficiency of various metal oxide nanostructures and nanocomposites

| Adsorbent | $Q_o$ (mg/g) | References |
|---|---|---|
| $MoS_2/WO_3$ composite | 268.42 | [35] |
| $W_{18}O_{49}$ nanostructure | 375.94 | [36] |
| CNC/ZnO nanocomposite | 64.93 | [37] |
| ZnO NPs | 143.6 | [38] |
| $TiO_2$/MgO/ZnO/biochar composites (BC-TMZ) | 114.5 | [39] |
| $MnO_2$/BC | 185.1 | [40] |
| MGO/CH NC | 332.6 | [41] |
| Core-shell activated carbon/CaO composites | 356 | [42] |
| Magnetic ball-milled BC (MBM-BC) | 500.5 | [43] |
| h-$MoO_3$ rod like microcrystal | 99.9 | [44] |
| Orthorhombic-$MoO_3$ | 152 | [45] |
| Orthorhombic-$MoO_3$ | 705.3 | This study |
| mp-$MoO_3$ | 729.8 | This study |

### 3.5. Industrial wastewater treatment

For the realistic treatment of wastewater, the sample was collected from textile industry in Ambala (Haryana). All the three adsorbent were used for the removal of colored substance from wastewater and the removal percentage is presented in Fig. 6. The adsorption condition maintained with continuous stirring at 30°C temperature, natural pH with 20 mg adsorbent dose,

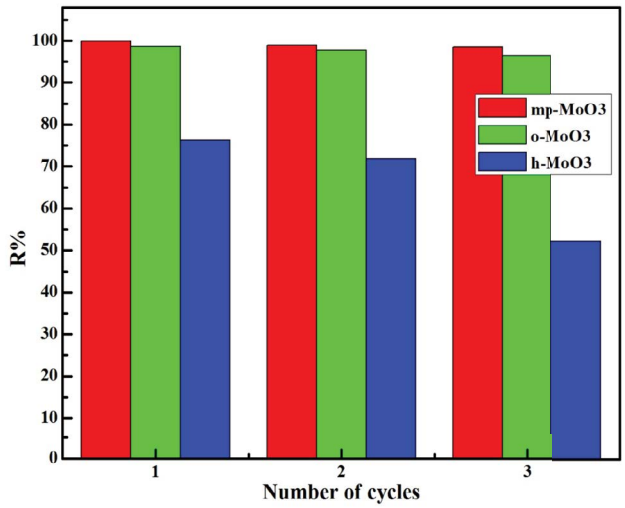


Fig. 5. Recyclability test corresponding to $MoO_3$ nanostructures.

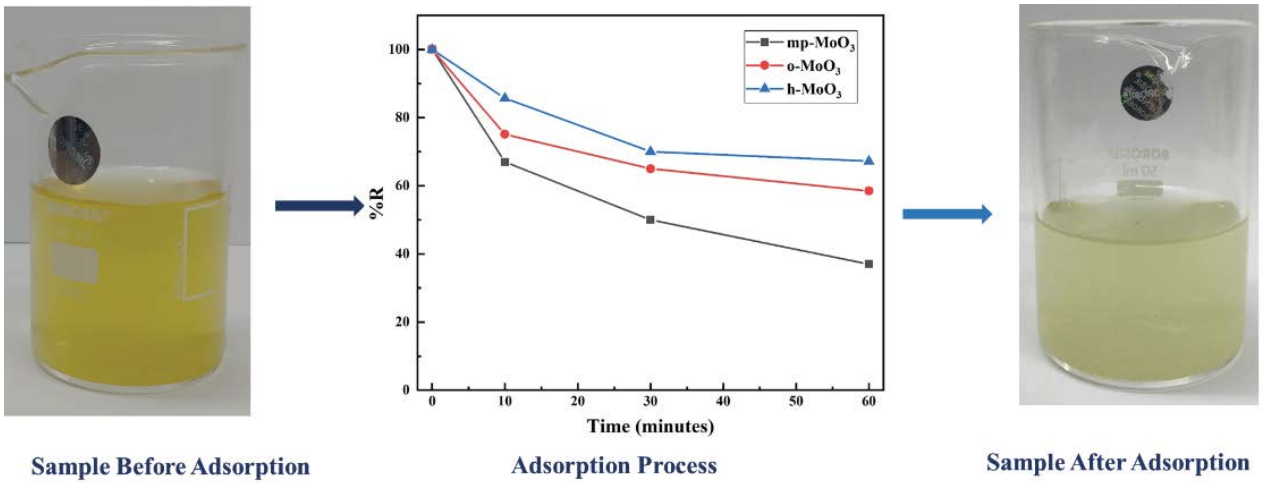


Fig. 6. Pollutant adsorption from industrial wastewater.

40 mL solution with a contact time of 60 min. The obtained results show that mp-$MoO_3$ followed higher %*R* followed by o-$MoO_3$ with least removal by h-$MoO_3$. On comparing the results with prepared MB solution in lab, the obtained removal efficiency is somewhat lower. It is because that industrial water contained various pollutants along with MB dye. These may be cationic as well as anionic in nature. Being an anionic nature of adsorbents, is not possible to remove anionic pollutants. Therefore, not complete removal of color from the solution was seen.

## 4. Conclusion

The effect of variation in the initial dye concentration on adsorption activity has been studied using three different phases of $MoO_3$. The h-$MoO_3$ is found to be less suitable for MB adsorption whereas mp-$MoO_3$ exhibits significantly higher removal efficiency. The removal rate of all samples decreases with increasing dye concentration because of the relative reduction in the adsorption sites. The removal efficiency was found to be increased from 67.5% to 99.4% with varying dye concentration in case of mp-$MoO_3$. Similar trend was obtained for o-$MoO_3$ with removal percentage 25.8% to 99%. However, h-$MoO_3$ exhibits lowest removal percentage from 4% to 28.2% only. Maximum experimental efficiency was found for mp-$MoO_3$ with value 633.1 mg/g followed by o-$MoO_3$ with value 425 mg/g. The adsorption was found to be following intraparticle diffusion kinetics which hints towards the diffusion of dye into the adsorbent surface. The isotherm models suggest that mp-$MoO_3$ possesses the highest adsorption efficiency followed by o-$MoO_3$ with value of 729.8 and 705.3 mg/g, respectively. Langmuir model better explains adsorption at lower temperature whereas enhanced adsorption at higher temperature is explained by Freundlich isotherms. The improvement of the reactive sites results in enhancement of adsorption at higher temperatures. The regeneration study shows that the removal capacity remains up to 98% for both mp-$MoO_3$ and o-$MoO_3$ after three cycles but reduced to around 50% from 75% in case of h-$MoO_3$. The $MoO_3$ nanostructure's noteworthy removal efficiency points to it as a potential adsorbent material.

## Acknowledgements

The author acknowledges the SERB, Department of Science and Technology, India for providing funds under research project (EEQ/2021/000933) and the financial support provided by Punjab University, Chandigarh for article processing charges.

## Conflict of interest

The authors declare that they have no known competing financial interests or personal relationships that could have appeared to influence the work reported in this paper.

## References

[1] M. Bhowmik, M. Kanmani, A. Debnath, B. Saha, Sono-assisted rapid adsorption of anionic dye onto magnetic $CaFe_2O_4$/$MnFe_2O_4$ nanocomposite from aqua matrix, Powder Technol., 354 (2019) 496–504.

[2] P. Das, P. Debnath, A. Debnath, Enhanced sono-assisted adsorptive uptake of malachite green dye onto magnesium ferrite nanoparticles: kinetic, isotherm and cost analysis, Environ. Nanotechnol. Monit. Manage., 16 (2021) 100506, doi: 10.1016/j.enmm.2021.100506.

[3] N. Kumar, T. Bahl, R. Kumar, Study of the methylene blue adsorption mechanism using $ZrO_2$/Polyaniline nanocomposites, Nano Express, 1 (2020) 030025, doi: 10.1088/2632-959X/abca10.

[4] R. Bhateria, D. Jain, Water quality assessment of lake water: a review, Water Resour. Manage., 2 (2016) 161–173.

[5] T.J. Al-Musawi, N. Mengelizadeh, O.A. Rawi, D. Balarak, Capacity and modeling of Acid Blue 113 dye adsorption onto chitosan magnetized by $Fe_2O_3$ nanoparticles, J. Polym. Environ., 30 (2022) 344–359.

[6] S. Benkhaya, S. M'rabet, A.E. Harfi, A review on classifications, recent synthesis and applications of textile dyes, Inorg. Chem. Commun., 115 (2020) 107891, doi: 10.1016/j.inoche.2020.107891.

[7] S. Benkhaya, S. M'rabet, A.E. Harfi, Classifications, properties, recent synthesis and applications of azo dyes, Heliyon, 6 (2020) e03271, doi: 10.1016/j.heliyon.2020.e03271.

[8] C. Belpaire, T. Reyns, C. Geeraerts, J.V. Loco, Toxic textile dyes accumulate in wild European eel *Anguilla Anguilla, Chemosphere, 138 (2015) 784–791.*

[9] L. Chungkrang, S. Bhuyan, A.R. Phukan, Natural dyes: extraction and applications, Int. J. Curr. Microbiol. Appl. Sci., 10 (2021) 1669–1677.

[10] M. Kagathara, D.J. Dalal, H.A. Solanki, Revealing explanation on organic dyes: a review, Int. J. Res. Advent Technol., 8 (2020) 1–8.

[11] M.A. Mohammed, A. Shitu, A. Ibrahim, Removal of methylene blue using low-cost adsorbent: a review, Res. J. Chem. Sci., 4 (2014) 91–102.

[12] E.O. Ezugbe, S. Rathilal, Membrane technologies in wastewater treatment: a review, Membranes, 10 (2020) 89, doi: 10.3390/membranes10050089.

[13] L.G.C. Villegas, N. Mashhadi, M. Chen, D. Mukherjee, K.E. Taylor, N. Biswas, A short review of techniques for phenol removal from wastewater, Curr. Pollut. Rep., 2 (2016) 157–167.

[14] P. Rajasulochana, V. Preethy, Comparison on efficiency of various techniques in treatment of waste and sewage water – a comprehensive review, Resour.-Effic. Technol., 2 (2016) 175–184.

[15] A.N. Chowdhury, A. Rahim, Y.J. Ferdosi, M.S. Azam, M.M. Hossain, Cobalt–nickel mixed oxide surface: a promising adsorbent for the removal of PR dye from water, Appl. Surf. Sci., 256 (2010) 3718–3724.

[16] H. Sadegh, G.A.M. Ali, V.K. Gupta, A.S.H. Makhlouf, R. Shahryari-Ghoshekandi, M.N. Nadagouda, M. Sillanpaa, E. Megiel, The role of nanomaterials as effective adsorbents and their applications in wastewater treatment, J. Nanostruct. Chem., 7 (2017) 1–14.

[17] M.S. Beltran, F.P. Delgado, R. Garcia, W.A. Flore, C.O. Gutierrez, A.S. Beltran, Fast methylene blue removal by $MoO_3$ nanoparticles, J. Mater. Sci.: Mater. Electron., 28 (2016) 2935–2948.

[18] D.O. Scanlon, G.W. Watson, D.J. Payne, G.R. Atkinson, R.G. Egdell, D.S.L. Law, Theoretical and experimental study of the electronic structure of $MoO_3$ and $MoO_2$, J. Phys. Chem. C, 114 (2010) 4636–4645.

[19] I.A. de-Castro, R.S. Datta, J.Z. Ou, A. Castellanos-Gomez, S. Sriram, T. Daeneke, K. Kalantar-Zadeh, Molybdenum oxides-from fundamental to functionality, Adv. Mater., 29 (2017) 170619–170649.

[20] A. Chthambararaj, N.R. Yogamalar, A.C. Bose, Hydrothermally synthesized h-$MoO_3$ and $\alpha$-$MoO_3$ nanocrystals: new findings on crystal-strcture-dependent charge transport, Cryst. Growth Des., 16 (2016) 1984–1995.

[21] Y. Song, Y. Zhao, Z. Huang, J. Zhao, Aqueous synthesis of molybdenum trioxide (h-$MoO_3$, $\alpha$-$MoO_3{\cdot}H_2O$ and *h*-/$\alpha$-$MoO_3$ composites) and their photochromic properties study, J. Alloys Compd., 693 (2017) 1290–1296.

[22] N. Kumar, R. Kumar, Efficient adsorption of methylene blue on hybrid structural phase of $MoO_3$ nanostructure,

Mater. Chem. Phys., 275 (2022) 125211, doi: 10.1016/j.matchemphys.2021.125211.
[23] A.K. Bhattacharya, T.K. Naiya, S.N. Mandal, S.K. Das, Adsorption, kinetics and equilibrium studies on removal of Cr(VI) from aqueous solutions using different low-cost adsorbents, Chem. Eng. J., 137 (2008) 529–541.
[24] R. Junejo, S. Memon, F.N. Memon, A.A. Memon, F. Durmaz, A.A. Bhatti, A.A. Bhatti, Thermodynamic and kinetic studies for adsorption of Reactive Blue (RB-19) dye using calix[4]arene-based adsorbent, J. Chem. Eng. Data, 8 (2020) 3407–3415.
[25] H. Moussout, H. Ahlafi, M. Aazza, H. Maghat, Critical of linear and non-linear equations of pseudo-first-order and pseudo-second-order kinetic models, Karbala Int. J. Mod. Sci., 4 (2018) 244–254.
[26] M. Zbair, Z. Anfar, H.A. Ahsaine, K. Hamza, Kinetics, equilibrium, statistical surface modeling and cost analysis of Paraquat removal from aqueous solution using carbonated jujube seed, RSC Adv., 9 (2019) 1084–1094.
[27] N. Abdus-Salam, F. Ugbe, V.A. Ikudayisi-Ugbe, Optimization and sorption isotherms analysis of anionic dye eosin yellow decontamination by goethite adsorbents, Acta Sci. Malaysia, 4 (2020) 51–57.
[28] G.K. Rajahmundry, C. Garlapati, P.S. Kumar, R.S. Alwi, D.V.N. Vo, Statistical analysis of adsorption isotherm models and its appropriate selection, Chemosphere, 276 (2021) 130176, doi: 10.1016/j.chemosphere.2021.130176.
[29] U.A. Edet, A.O. Ifelebuegu, Kinetics, isotherms, and thermodynamic modeling of the adsorption of phosphates from model wastewater using recycled brick waste, Processes, 8 (2020) 665, doi: 10.3390/pr8060665.
[30] E.C. Nnadozie, P.A. Ajibade, Data for experimental and calculated values of the adsorption of Pb(II) and Cr(VI) on APTES functionalized magnetite biochar using Langmuir, Freundlich and Temkin equations, Data Brief, 32 (2020) 106292, doi: 10.1016/j.dib.2020.106292.
[31] S.M. Bassir, S.R. Shadizadeh, Static adsorption of a new cationic biosurfactant on carbonate minerals: application to EO, Pet. Sci. Technol., 38 (2020) 462–471.
[32] A.O. Dada, A.P. Olalekan, A. Olatunya, O. Dada, Langmuir, Freundlich, Temkin and Dubinin–Radushkevich isotherms studies of equilibrium sorption of $Zn^{2+}$ unto phosphoric acid modified rice husk, IOSR J. Appl. Chem., 3 (2012) 38–45.
[33] Q. Hu, Z. Zhang, Application of Dubinin–Radushkevich isotherm model at the solid/solution interface: a theoretical analysis, J. Mol. Liq., 277 (2019) 646–648.
[34] A.H. Jawad, A.S. Abdulhameed, Mesoporous Iraqi red kaolin clay as an efficient adsorbent for methylene blue dye: adsorption kinetic, isotherm and mechanism study, Surf. Interfaces, 18 (2020) 100422, doi: 10.1016/j.surfin.2019.100422.
[35] Y. Zheng, J. Wang, Y. Wang, H. Zhou, Z. Pu, Q. Yang, W. Huang, The combination of $MoS_2/WO_3$ and its adsorption properties of methylene blue at low temperatures, Molecules, 25 (2020) 2, doi: 10.3390/molecules25010002.
[36] Y. Shang, X. Cheng, R. Shi, Q. Ma, Y. Wang, P. Yang, Synthesis and comparative investigation of adsorption capability and photocatalytic activities of $WO_3$ and $W_{18}O_{49}$, Mater. Sci. Eng., B, 262 (2020) 114724, doi: 10.1016/j.mseb.2020.114724.
[37] O.A. Oyewo, A. Adeniyi, B.B. Sithole, M.S. Onyango, Sawdust-based cellulose nanocrystals incorporated with ZnO nanoparticles as efficient adsorption media in the removal of methylene blue dye, ACS Omega, 5 (2020) 18798–18807.
[38] H. Kahsay, Synthesis and characterization of ZnO nanoparticles using aqueous extract of *Becium grandiflorum* for antimicrobial activity and adsorption of methylene blue, Appl. Water Sci., 11 (2021) 45, doi: 10.1007/s13201-021-01373-w.
[39] S. Zhai, M. Li, D. Wang, L. Zhang, Y. Yang, S. Fu, *In-situ* loading metal oxide particles on bio-chars: reusable materials for efficient removal of methylene blue from wastewater, J. Cleaner Prod., 220 (2019) 460–474.
[40] S.I. Siddiqui, O. Manzoor, M. Mohsin, S.A. Chaudhry, Nigella sativa seed-based nanocomposites-$MnO_2$/BC: an antibacterial material for photocatalytic degradation, and adsorptive removal of methylene blue from water, Environ. Res., 171 (2019) 328–340.
[41] D. Gautam, S. Hooda, Magnetic graphene oxide/chitin nanocomposites for efficient adsorption of methylene blue and crystal violet from aqueous solutions, J. Chem. Eng. Data, 65 (2020) 4052–4062.
[42] M.M. Emara, R.S. Farag, M.F. Mubarak, S.K. Ali, Synthesis of core–shell activated carbon/CaO composite from *Ficus nitida* leaves, as an efficient adsorbent for removal of methylene blue, Nanotechnol. Environ. Eng., 5 (2020) 24, doi: 10.1007/s41204-020-00088-8.
[43] Y. Li, A.R. Zimmerman, F. He, J. Chen, L. Han, H. Chen, X. Hu, B. Gao, Solvent-free synthesis of magnetic biochar and activated carbon through ball-mill extrusion with $Fe_3O_4$ nanoparticles for enhancing adsorption of methylene blue, Sci. Total Environ., 722 (2020) 137972, doi: 10.1016/j.scitotenv.2020.137972.
[44] M.L.D. Sa, F.X. Nobre, L.D.S. Silva, G.D.S. Sousa, M.L. Takeno, E.A.A. Junior, J.M.E.D. Matos, M.R.M.E.D. Santos, Preparation of new h-$MoO_3$ rod-like microcrystals for effective removal of cationic dye in aqueous solution, Int. J. Environ. Res., 15 (2021) 105–124.
[45] S. Rakass, H.O. Hassani, M. Abboudi, F. Kooli, A. Mohmoud, A. Aljuhani, F.A. Wadaani, Molybdenum trioxide: efficient nanosorbent for removal of methylene blue dye from aqueous solutions, Molecules, 23 (2018) 2295–2312.